Atmos. Chem. Phys. Discuss., https://doi.org/10.5194/acp-2018-1139
Manuscript under review for journal Atmos. Chem. Phys.
Discussion started: 6 November 2018

Atmospheric Chemistry and Physics Discussions

Large-eddy simulation of radiation fog with comprehensive two-moment bulk microphysics: Impact of different aerosol activation and condensation parameterizations

Johannes Schwenkel[1] and Björn Maronga[1,2]

[1]Institute of Meteorology and Climatology, Leibniz Universität Hannover, Hannover, Germany
[2]Geophysical Institute, University of Bergen, Bergen, Norway

Correspondence to: Johannes Schwenkel (schwenkel@muk.uni-hannover.de)

Abstract. In this paper we study the influence of the cloud microphysical parameterization on large-eddy simulations of radiation fog. A deep fog case as observed at Cabauw (Netherlands) is investigated using high-resolution large-eddy simulations with different microphysics treatments for activation and diffusional growth. A comparison of the results indicates that the commonly applied assumption of saturation adjustment produces at maximum 6.9% higher liquid water paths compared to the explicit diffusional growth method but has no significant influence on the general life cycle of the fog layer. Differences are found to be the most pronounced at the top of the fog layer where the highest supersaturations occurs. Furthermore, the effect of different droplet number concentrations is investigated by using a selection of common activation schemes. We find, in line with previous studies, a positive feedback between the droplet number concentration and both the optical thickness and the strength of the fog layer. Furthermore, we perform an explicit analysis of the budgets of condensation, evaporation, sedimentation and advection in order to assess which processes have the largest spatial and temporal influence on the development of the fog layer.

1 Introduction

The prediction of fog is an important part of the estimation of hazards and efficiency in traffic and economy (Bergot, 2013). The annual damage caused by fog events is estimated to be the same as the amount caused by winter storms (Gultepe et al., 2009). Despite improvements in numerical weather prediction (NWP) models, the quality of fog forecasts is still unsatisfactory. The explanation for this is obvious: fog is a meteorological phenomenon influenced by a multitude of complex physical processes. Namely, these processes are radiation, turbulence, atmosphere-surface interactions, and cloud microphysics, and which interact on different scales (e.g. Gultepe et al., 2007; Haeffelin et al., 2010). The key issue for improving fog prediction in NWP models is to either resolve all relevant processes, or to parameterize them appropriately.

In recent years various studies have focused on the influence of microphysics on fog. In particular, the activation of aersols, which determines how many aerosols at a certain supersaturation get activated and hence can grow into cloud drops, is of major interest (e.g. Bott, 1991; Hammer et al., 2014; Boutle et al., 2018).

Atmos. Chem. Phys. Discuss., https://doi.org/10.5194/acp-2018-1139
Manuscript under review for journal Atmos. Chem. Phys.
Discussion started: 6 November 2018

Atmospheric Chemistry and Physics Discussions

Stolaki et al. (2015) investigated and compared the influence of aerosols on the life cycle of a radiation fog event while using two-dimensional large-eddy simulations (LESs) with a two-moment warm microphysics scheme after Geoffroy et al. (2008) and Khairoutdinov and Kogan (2000) and included an activation parameterization after Cohard et al. (1998). In other fog studies, using single-column models, different activation schemes such as the simple Twomey-power law activation in Bott and Trautmann (2002) and the scheme of Abdul-Razzak and Ghan (2000) (see Zhang et al., 2014) were applied. Furthermore, also more advanced methods such as sectional models have been used for an appropriate activation representation. Maalick et al. (2016) used the SALSA module in two-dimensional studies for a size-resolved activation. This large number of different activation parameterizations raises the question of the quantitative differences between the individual methods. Furthermore, schemes that parameterize activation based on updrafts might fail for fog. Such schemes derive supersaturation as as a function of vertical velocity, which is valid for common clouds, but not for radiation fog, which is mainly driven by longwave radiative cooling (Boutle et al., 2018).

Although great progress has been made to understand different microphysical processes in radiation fog based on numerical experiments, turbulence as a key process has been either fully parameterized (single-column models) or oversimplified (two-dimensional LES). Since turbulence is a fundamentally three-dimensional process, the full complexity of all relevant mechanisms can only be reproduced with three-dimensional LESs (Nakanishi, 2000).

Moreover, a disadvantage of the most former studies is the use of saturation adjustment, which implies that supersaturations are immediately removed within one time step. This approach is only valid when the time scale for diffusion of water vapour (on order of 2-5 s) is much smaller than the model time step, which is the case in large scale models where time steps are on the order of 1 min. However, in LES (as in the present study), the time step easily goes down to split seconds so that this assumption is violated and might lead to excessive condensation (e.g. Lebo et al., 2012).

This paper addresses two issues related to the microphysics parameterization in numerical models to simulate radiation fog. Firstly, the error introduced by using saturation adjustment for simulating fog in LES models will be analyzed and compared with an explicit approach for diffusional growth. Secondly, the influence of different numbers of activated aerosol by using different Twomey-based activation schemes on the simulated fog layer is investigated with the focus on feedback effects with the fog microphysics.

2 Methods

This section will outline the used LES model and the treatment of radiation and land-surface interactions, followed by a more detailed description of the bulk microphysics implemented in the Parellized Large-Eddy Simulation Model (PALM) and the extensions made in the scope of the present study.

2.1 LES model with embedded radiation and land surface model

In this study the LES model PALM (Maronga et al. 2015; revision 2675) was used. PALM has been successfully applied to simulate the stable boundary layer (BL) (e.g. during the first intercomparison of LES for stable BL, GABLS, Beare et al.,

Atmos. Chem. Phys. Discuss., https://doi.org/10.5194/acp-2018-1139
Manuscript under review for journal Atmos. Chem. Phys.
Discussion started: 6 November 2018

Atmospheric Chemistry and Physics Discussions

2006) as well as radiation fog (Maronga and Bosveld, 2017). The model is based on the non-hydrostatic incompressible Boussinesq-approximated Navier-Stokes equations, and prognostic equations for total water mixing ratio, potential temperature, and subgrid-scale turbulence kinetic energy.

In order to account for radiative effects on fog and the Earth's surface energy balance, the radiation code RRTMG (Clough et al., 2005) has been recently coupled to PALM, running as an independent single column model for each vertical column of the LES domain. RRTMG calculates the radiative fluxes (shortwave and longwave) for each grid volume while considering profiles of pressure, temperature, humidity, liquid water and the droplet number concentration (n_c). Compared to the precursor study of Maronga and Bosveld (2017), improvements in the microphysics parameterization introduced in the scope of the present study allow a more realistic calculation of the fog's radiation budget, since n_c is now represented as a prognostic quantity instead of the previously fixed value. Radiation calculations traditionally require enormous computation time, the radiation code is called at fixed intervals on the order of 1 min only.

Moreover, PALM's land surface model (LSM) is used to calculate the surface fluxes of sensible and latent heat. The LSM consists of multi-layer soil model, predicting soil temperature and soil moisture, as well as a solver for the energy balance of the Earth's surface using a resistance parameterization. The implementation is based on the ECMWF-IFS land surface parametrization (H-TESSEL) and its adaptation in the DALES model (Heus et al., 2010). A description of the LSM and a validation of the model system for radiation fog is given in Maronga and Bosveld (2017).

2.2 Bulk microphysics

As a part of this study, the two-moment microphysics scheme of Seifert and Beheng (2001; 2006) implemented in PALM, which basically only predicts the rain droplet number concentration (n_r) and cloud water mixing (q_r) is extended by prognostic equations for n_c and cloud water mixing ratio (q_c). The scheme of Seifert and Beheng (2001; 2006) is based on the separation of the cloud and rain droplet scale by using a radius threshold of 40 µm. This separation is mainly used for parameterizing coagulation processes by assuming different distribution functions for cloud and rain droplets. However, as collision and coalescence are weak in fog due to small average droplet radii, the production of rain droplets is negligible. Consequently, only the number concentration and mixing ratio of droplets (containing all liquid water and thus abbreviated with q_l here) are considered in the following. The budgets of the cloud water mixing ratio and number concentration are given by

$$\frac{\partial q_\mathrm{l}}{\partial t} = -\frac{\partial u_i q_\mathrm{l}}{\partial x_i} + \left(\frac{\partial q_\mathrm{l}}{\partial t}\right)_\mathrm{activ} + \left(\frac{\partial q_\mathrm{l}}{\partial t}\right)_\mathrm{cond} - \left(\frac{\partial q_\mathrm{l}}{\partial t}\right)_\mathrm{auto} - \left(\frac{\partial q_\mathrm{l}}{\partial t}\right)_\mathrm{accr} - \left(\frac{\partial q_\mathrm{l}}{\partial t}\right)_\mathrm{sedi}, \tag{1}$$

$$\frac{\partial n_\mathrm{c}}{\partial t} = -\frac{\partial u_i n_\mathrm{c}}{\partial x_i} + \left(\frac{\partial n_\mathrm{c}}{\partial t}\right)_\mathrm{activ} - \left(\frac{\partial n_\mathrm{c}}{\partial t}\right)_\mathrm{evap} - \left(\frac{\partial n_\mathrm{c}}{\partial t}\right)_\mathrm{auto} - \left(\frac{\partial n_\mathrm{c}}{\partial t}\right)_\mathrm{accr} - \left(\frac{\partial n_\mathrm{c}}{\partial t}\right)_\mathrm{sedi}. \tag{2}$$

The terms on the right-hand side represent the decrease or increase by advection, activation, diffusional growth, autoconversion, accretion, and sedimentation (from left to right). Following Ackerman et al. (2009), cloud water sedimentation is parameterized assuming that droplets are having a log-normal distribution and following a Stokes regime. This results in a sedimentation flux

Atmos. Chem. Phys. Discuss., https://doi.org/10.5194/acp-2018-1139
Manuscript under review for journal Atmos. Chem. Phys.
Discussion started: 6 November 2018

of

$$F_{q_l} = k\left(\frac{4}{3}\pi\rho_l n_c\right)^{-2/3}(\rho q_l)^{\frac{5}{3}}\exp(5\ln^2\sigma_g), \tag{3}$$

with ρ_l being density of water, the parameter $k = 1.2\times10^8$ m^{-1}s^{-1}, and σ_g=1.3 the geometric standard deviation of the droplet distribution (Geoffroy et al., 2010). The main focus of this paper is to investigate the influence of different microphysical parameterizations of activation and condensation processes on microphysical and macroscopic properties of radiation fog. Those different activation and condensation parameterizations will be discussed in the following.

2.2.1 Activation

It is well known that the aerosol distribution and the activation process are of great importance to the life cycle of fog (e.g. Gultepe et al., 2007). The amount of activated aerosols determines the number concentration of droplets within the fog, which in turn has a significant influence on radiation through optical thickness as well as on sedimentation and consequently influences macroscopic properties of the fog, such as its vertical extension. For these reasons, a sophisticated treatment of the activation process is an essential prerequisite for the simulation of radiation fog. Several parameterizations for bulk microphysics models have been developed to provide a realistic activation model. In this work, three of these activation schemes will be compared with each other in order to quantify their influence on the development of a radiation fog event. The schemes considered in this scope are the simple activation scheme of Twomey (1959) which was used, e.g., by Bott and Trautmann (2002) to simulate radiation fog, the scheme of Cohard et al. (1998) (used by e.g. Stolaki et al., 2015; Mazoyer et al., 2017) and the one by Khvorostyanov and Curry (2006). The latter two represent an empirical and analytically extension of Twomeys scheme, respectively. Consequently, these parameterizations are frequently termed Twomey-type parameterizations with the general type of

$$N_{\mathrm{CCN}}(s) = N_0 s^k, \tag{4}$$

where N_{CCN} are the number of activated cloud condensation nuclei (CCN), N_0 and k are parameters depending on the aerosol distribution, and s is the supersaturation. This equation can be solved using several approaches and mathematical complexity levels. In the following, these three schemes and their underlying equations are presented.

1. **Twomey (1959):** The simple power law expression (see Eq. 4) is well known and has been used for decades to estimate the number of activated aerosol for a given air mass in dependence of the supersaturation. A weakness of this approach is that the parameters N_0 and k are usually assumed to be constant and are not directly linked to the microphysical properties. Furthermore, this relationship creates an unbounded number of CCN at high supersaturations.

2. **Cohard et al. (1998):** extended Twomey's power law expression by using a more realistic four-parameter CCN activation spectrum as shaped by the physiochemical properties of the accumulation mode. Although an extension to the multi-modal representation of an aerosol spectrum would be possible, all relevant aerosols that are activated in typical supersaturations within clouds and especially fog are represented in the accumulation mode (Cohard et al., 1998; Stolaki

et al., 2015). Following Cohard et al. (1998) and Cohard and Pinty (2000) the activated CCN number concentration is expressed by

$$N_{\mathrm{CCN}}(s) = Cs^k \times F\left(\mu, \frac{k}{2}, \frac{k}{2}+1; \beta s^2\right) \tag{5}$$

while C is proportional to the total number concentration of CCN that is activated when supersaturation s tends to infinity. Parameters k, μ, and β are adjustable shape parameters associated with the characteristics of the aerosol size spectrum such as geometric mean radius and the geometric standard deviation as well as with chemical composition and solubility of the aerosols. Thus, in contrast to a simple Twomey approach, the influence of physiochemical properties of the aerosol spectrum are taken into account.

3. **Khvorostyanov and Curry (2006):** have found an analytical solution to express the activation spectrum using Koehler theory. Therein, it is assumed that the dry aerosol spectrum follows a log-normal size distribution of aerosol f_d:

$$f_d = \frac{dN_a}{dr_{\mathrm{d}}} = \frac{N_{\mathrm{t}}}{\sqrt{2\pi}\ln\sigma_{\mathrm{d}} r_{\mathrm{d}}} \exp\left[-\frac{\ln^2(r_{\mathrm{d}}/r_{\mathrm{d0}})}{2\ln^2\sigma_{\mathrm{d}}}\right]. \tag{6}$$

Here, r_{d} is the dry aerosol radius, N_{t} the total number of aerosols, σ_d is the dispersion of the dry aerosol spectrum, and r_{d0} is the mean radius of the dry particles. The number of activated CCN as a function of supersaturation s is then given by

$$N_{\mathrm{CCN}}(s) = \frac{N_{\mathrm{t}}}{2}[1 - \mathrm{erf}(u)]; \qquad u = \frac{\ln(s_0/s)}{\sqrt{2}\ln\sigma_{\mathrm{s}}}, \tag{7}$$

where erf is the Gaussian error function, and

$$s_0 = r_{\mathrm{d0}}^{-(1+\beta)}\left(\frac{4A^3}{27b}\right)^{1/2}, \qquad \sigma_s = \sigma_{\mathrm{d}}^{1+\beta}. \tag{8}$$

In this case, A is the Kelvin parameter and b and β depend on the chemical composition and physical properties of the soluble part of the dry aerosol.

Since prognostic equations are neither considered for the aerosols nor their sources and sinks, a fixed aerosol background concentration is prescribed by setting parameters N_0, C and N_{t} for the three activation schemes. The different nomenclature of the aerosol background concentration is based on the nomenclature used in the original literature.

The activation rate is then calculated as

$$\left(\frac{\partial n_{\mathrm{c}}}{\partial t}\right)_{activ} = \max\left(\frac{N_{\mathrm{CCN}} - n_{\mathrm{c}}}{\Delta t}, 0\right), \tag{9}$$

where n_{c} is the number of previously activated aerosols that are assumed to be equal to the number of pre-existing droplets and Δt is the length of the model time step. It should be noted that this method does not represent the reduction of CCN. However, this error can be neglected since processes as aerosol washout and dry deposition are of minor importance for radiation fog. For all activation schemes it is assumed that every activated CCN becomes a droplet with an initial radius of 1 µm. This results

Atmos. Chem. Phys. Discuss., https://doi.org/10.5194/acp-2018-1139
Manuscript under review for journal Atmos. Chem. Phys.
Discussion started: 6 November 2018

in a change of liquid water, which is considered by the condensation scheme and is described in the next section. Furthermore, we performed a sensitivity study with initial radii of 0.5 µm to 2 µm, which showed that the choice of the initial radius had no impact on the results (not shown). This is consistent with the findings of Khairoutdinov and Kogan (2000) and Morrison and Grabowski (2007).

2.2.2 Condensation

The representation of diffusional growth and evaporation is one of the fundamental tasks of cloud physics. In many microphysical models, a saturation adjustment scheme is applied. The basic idea of this scheme is that all supersaturation is removed within one model time step and supersaturations are thus neglected. Despite the many years of application of this scheme, its influence on microphysical processes is discussed controversially in the community (e.g. Morrison and Grabowski, 2008; Thouron et al., 2012; Lebo et al., 2012). Saturation adjustment might hence especially be a source of error in fog simulations where very small time steps are used due to small grid spacings as outlined earlier. In the following, both the saturation adjustment scheme and the explicit supersaturation calculation are presented.

1. **Saturation adjustment:** Using the saturation adjustment scheme, q_l represents a diagnostic value calculated by means of

$$q_\mathrm{l} = \max(0, q - q_\mathrm{r} - q_\mathrm{s}), \tag{10}$$

where q is the total water mixing ratio, and q_s is the saturation mixing ratio. The saturation mixing ratio, which is a function of temperature, is approximated in a first step by

$$q_\mathrm{s}(T_\mathrm{l}) = \frac{R_\mathrm{d}}{R_\mathrm{v}} \frac{e_\mathrm{s}(T_\mathrm{l})}{p - e_\mathrm{s}(T_\mathrm{l})}, \tag{11}$$

where T_l is the liquid water temperature and p the pressure. The individual gas constants for dry air and water vapor are denoted R_d and R_v, respectively. For the saturation vapor pressure e_s an empirical relationship of Bougeault (1981) is used. In a second step q_s is corrected using a first-order Taylor series expansion of q_s:

$$q_\mathrm{s}(T) = q_\mathrm{s}(T_\mathrm{l}) \frac{1 + \beta q}{1 + \beta q_\mathrm{s}(T_\mathrm{l})}, \tag{12}$$

with

$$\beta = \frac{L_\mathrm{v}}{R_\mathrm{v} c_\mathrm{p} T_\mathrm{l}^2}, \tag{13}$$

where c_p is the specific heat of dry air and L_v is the latent heat of vaporization. As aforementioned, in each model time step, all supersaturation is converted into liquid water or, in subsaturated regions, the liquid water is reduced until saturation.

2. **Explicit supersaturation calculation:** Supersaturation is calculated explicitly from the predicted water vapor mixing ratio q_v and the temperature T (from which q_s can be derived). However, since it is assumed that the supersaturation is

Atmos. Chem. Phys. Discuss., https://doi.org/10.5194/acp-2018-1139
Manuscript under review for journal Atmos. Chem. Phys.
Discussion started: 6 November 2018

Atmospheric Chemistry and Physics Discussions

kept constant during one model time step, the explicit approach requires a very small model time step of

$$\Delta t \leq 2\tau, \tag{14}$$

due to stability reasons (Árnason and Brown Jr, 1971). Here, τ is the supersaturation relaxation time which is approximated by

$$\tau \approx (4\pi D n_c \langle r \rangle)^{-1}, \tag{15}$$

where $\langle r \rangle$ is the average radius, and D the diffusivity of water vapor in air. Due to the low dynamic time step in the present study imposed by the Courant-Friedrichs-Lewy criterion (on the order of 0.1 s), however, the condensation time criterion is fulfilled. The rate of cloud water change due to condensation or evaporation is given by

$$\left(\frac{\partial q_\mathrm{l}}{\partial t}\right)_\mathrm{cond} = \frac{4\pi G(T,p)\rho_\mathrm{w}}{\rho_\mathrm{a}} s \int_0^\infty r f(r) dr \tag{16}$$

$$= \frac{4\pi G(T,p)\rho_\mathrm{w}}{\rho_\mathrm{a}} s r_\mathrm{c} \tag{17}$$

where r_c is the integral radius and $G = \frac{1}{F_\mathrm{K}+F_\mathrm{D}}$ included the thermal conduction and the diffusion of water vapor (Khairoutdinov and Kogan, 2000). The density ratio of liquid water and the solute is given by $\rho_\mathrm{w}/\rho_\mathrm{a}$.

Using such a small time step allows the use of a diagnostic approach for the supersaturation calculation. Nevertheless, pseudo-prognostic solutions are also used for the saturation calculation, which are able to mitigate the problem of spurious cloud-edge supersaturations (Grabowski and Morrison, 2008). Here, the error of these supersaturations, which tends to diminish with decreasing grid spacing and increasing advection velocity, can be considered to be small due to the relatively small grid spacing and relatively strong wind used in the present study (see next section).

3 Case description and model setup

The simulations performed in the present study are based on an observed deep fog event during the night from 22 to 23 March 2011 at the Cabauw Experimental Site for Atmospheric Research (CESAR). The fog case is described in detail in Boers et al. (2013) and was used as validation case for PALM in Maronga and Bosveld (2017). The CESAR site is dominated by rural grassland landscape and, although it is relatively close to the sea, there are typically continental aerosol conditions characterized by agricultural processes (Mensah et al., 2012).

The fog initially formed at midnight (as a thin near-surface layer), induced by radiative cooling, which also produced a strong inversion with a temperature gradient of 6 K between the surface and the 200 m tower-level. In the following the fog layer began to develop: At 0300 UTC the fog had a vertical extension of below 20 m increased to a fog top of 80-140 m at 0600 UTC. At this point, also the visibility was reduced to 100 m. After sunset which took place at 0545 UTC a further development was suppressed, which led to an effective evaporation of the fog due to direct solar heating of the surface. For details, see Boers et al. (2013).

Atmos. Chem. Phys. Discuss., https://doi.org/10.5194/acp-2018-1139
Manuscript under review for journal Atmos. Chem. Phys.
Discussion started: 6 November 2018

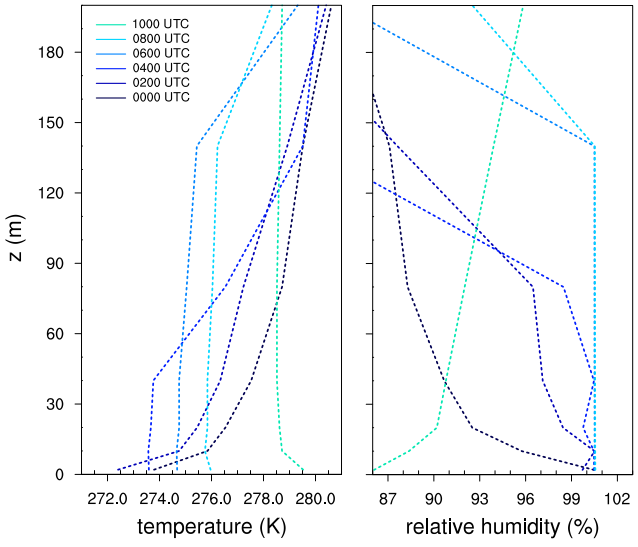

Figure 1. Profiles of potential temperature and relative humidity at different times as observed at Cabauw.

The model was initialized as described in the precursor study of Maronga and Bosveld (2017). Profiles of temperature and humidity (see Fig. 1) were derived from the CESAR 200 m-tower and used as initial profiles in PALM. A geostrophic wind of 5.5 m s^{-1} was prescribed based on the observed value at Cabauw at 0000 UTC.

The land surface model is initialized with short grassland as surface type and four soil model layers at the depths of 0.07 m, 0.28 m, 1.0 m and 2.89 m. The measured surface layer temperatures are interpolated to the respective levels, resulting in temperatures of 279.54, 279.60, 279.16, and 279.16 K for soil layers one to four, respectively. Furthermore, the initial soil moisture is set to the value at field capacity (0.491 m^{3}m^{-3}), which reflects the very wet soil and low water table in the Cabauw area. The heat conductivity was set to $\Lambda = 4$, based on the radiation and energy balance observed at 0000 UTC at Cabauw. Moreover, the roughness length for momentum was prescribed to 0.15 m. Note that Maronga and Bosveld (2017) discussed that this value appears to be a little high given the season and wind direction. For the purpose of the present study, this does, however not affect the purpose of the present study.

The radiation model starts at 0000 UTC and uses a time step of 60 s, which is a good compromise between saving computational time and accuracy of the radiative fluxes and heating rates.

All simulations start at 0000 UTC, before fog formation, and end at 1015 UTC on the next morning after the fog layer has fully dissipated. Precursor runs are conducted for additional 25 min using the initial state at 0000 UTC, but without radiation scheme and LSM in order to allow the development of turbulence in model without introducing feedbacks during that time (see Maronga and Bosveld, 2017).

Based on sensitivity studies of Maronga and Bosveld (2017), a grid spacing of $\Delta = 1$ m is adopted for all simulations, with a model domain size of 768 x 768 x 384 grid points in x-, y-, and z-direction, respectively. A sponge layer was used starting at a height of 344 m in order to prevent gravity waves to be reflected at the top boundary of the model.

Atmos. Chem. Phys. Discuss., https://doi.org/10.5194/acp-2018-1139
Manuscript under review for journal Atmos. Chem. Phys.
Discussion started: 6 November 2018

Atmospheric Chemistry and Physics Discussions

Table 1. Overview of conducted simulations. The droplet number concentration n_c is only given for simulations without activation scheme. In the simulations N1-N3 n_c is a prognostic quantity and thus variable in time and space. The aerosol background concentration is abbreviated with $N_{a,tot}$, and used to initialize the activation schemes. Note for the scheme of (Cohard et al., 1998) a conversion to the parameter C must be applied, while for both other activation schemes this value is directly used to prescribe N_0 and N_t, respectively.

#	Simulation	Activation scheme	n_c [cm^{-3}]	$N_{a,tot}$ [cm^{-3}]	Condensation scheme
1	REF	none	150	none	saturation-adjustment
2	C1	none	150	none	explicit
3	N1	Twomey (1959)	not fixed	842	explicit
4	N2	Cohard et al. (1998)	not fixed	842	explicit
5	N3	Khvorostyanov and Curry (2006)	not fixed	842	explicit

Tab.1 gives on overview over the simulation cases. All cases are initialized with (identical) continental aerosol conditions. Case REF represents a reference run with no activation scheme and thus a prescribed constant value of n_c =150 cm^{-3} (estimated from simulations of Boers et al. (2013)). This case represents a similar setup to the one described in Maronga and Bosveld (2017). Condensation processes are here treated with the saturation adjustment scheme (Seifert et al., 2006). In order to evaluate the influence of saturation adjustment on the development of radiation fog, identical assumptions are made in case C1, except that diffusion growth is calculated with the explicit method (see section 2.2.2). Cases N1-N3 use the activation schemes described in chapter 2.2.1. To ensure comparability between the different schemes, all of them are initialized with a continental aerosol background described in Cohard et al. (1998) which is characterized by an aerosol with the chemical composition of ammonium sulfate [$(NH_4)_2SO_4$], a background aerosol concentration of 842 cm^{-3}, a mean dry aerosol radius of $r_{d0} = 0.0218$ µm, and a dispersion parameter of the dry aerosol spectrum of $\sigma_d = 3.19$. For the Twomey activation scheme this results in $N_0 = 842$ cm^{-3} and $k = 0.8$ which is a typical value for the exponent for continental air masses (e.g. Pruppacher and Klett, 1997, page 289 ff). The Twomey activation scheme does not allow for taking aerosol properties into account. In contrast, the activation scheme of Cohard et al. (1998) requires the parameters C, k, β and μ to be derived from the aerosol properties. Here, values of $C = 2.1986 \cdot 10^6$ cm^{-3}, $k = 3.251$, $\beta = 621.689$ and $\mu = 2.589$ are used as described in Cohard and Pinty (2000). Finally, the activation scheme of Khvorostyanov and Curry (2006) can directly consider the aerosol properties, which are prescribed as aforementioned. Since changing other microphysical properties (such as mean geometric radius, chemical composition, or dispersion of dry aerosol spectrum) will have a similar effect to the physical outcomes as the variation of the aerosol concentration (because only cloud number concentration is affected), further simulation cases are omitted.

Atmos. Chem. Phys. Discuss., https://doi.org/10.5194/acp-2018-1139
Manuscript under review for journal Atmos. Chem. Phys.
Discussion started: 6 November 2018

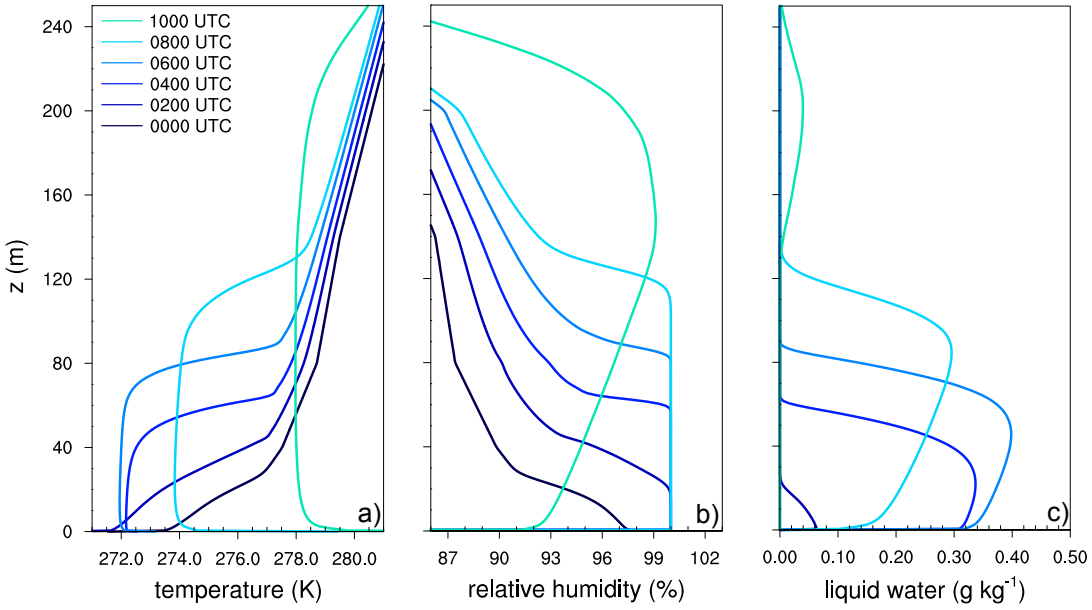

Figure 2. Profiles of potential temperature (a), relative humidity (b) and liquid water mixing ratio (c) at different times for the reference case REF.

4 Results

4.1 General fog life cycle and macrostructure

The reference case REF is conducted with a constant droplet number concentration of $n_c = 150\,\mathrm{cm}^{-3}$. The deepening of the fog layer can be seen in Fig 2, which shows the profiles of the potential temperature, relative humidity and liquid water mixing ratio at different times.

The fog onset is at 0055 UTC, defined by a visibility below 1000 m and a relative humidity of 100%. In the following the fog layer deepens and extends to a top of approximately 20 m at 0200 UTC. However, at this point the stratification of the layer is still stable with a temperature gradient of 6 K between the surface and the fog top. The persistent radiative cooling of the surface and the fog layer leads to a further vertical development of the fog, which is accompanied with a regime transition from stable to convective conditions within the fog layer (see Fig. 2a). This starts as soon as the fog layer begins to become optically thick (at 0330 UTC), and when radiative cooling at the fog top becomes the dominant process, creating a top-down convective boundary layer. The highest liquid water mixing ratio of $q_l = 0.41\,\mathrm{g\,kg}^{-1}$ is achieved at 0600 UTC at a height of 60 m (see Fig. 2c), while the the fog layer in total reaches the maximum one hour later at 0700 UTC. The lifting of the fog, which is defined by a non-cloudy near-surface layer ($q_l \leq 0.01\,\mathrm{g\,kg}^{-1}$), occurs at 0845 UTC. At 1130 UTC the fog is completely dissipated.

Atmos. Chem. Phys. Discuss., https://doi.org/10.5194/acp-2018-1139
Manuscript under review for journal Atmos. Chem. Phys.
Discussion started: 6 November 2018

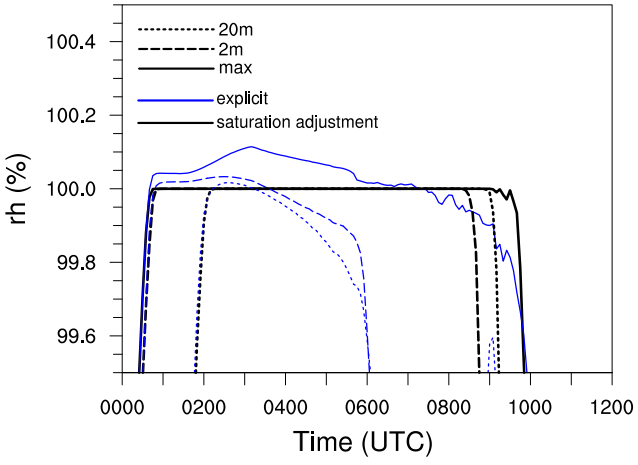

Figure 3. Time series of height averaged relative humidity/supersaturation at height levels of 2 m (dotted) and 20 m (dashed) as well as the domain wide maximum (solid) for cases REF and C1.

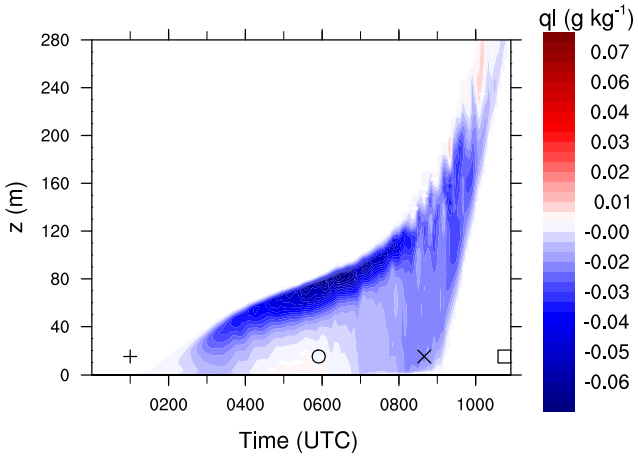

Figure 4. Absolute difference of liquid water mixing ratio from the C1 minus REF. Time marks of formation, maximum liquid water content, lifting, and dissipation are marked by plus signs, circles, crosses, and squares, respectively.

4.2 Saturation adjustment vs. explicit condensation

In this section we discuss the error introduced when using a saturation adjustment scheme for the simulation of radiation fog. For this, we compare two simulations with almost identical setup (cases Ref and C1). Activation is neglected in both cases and the n_c is set to a constant value of $150\,\mathrm{cm}^{-3}$. Due to the small grid spacing of 1 m used in our simulations, the time steps are on the order of 10^{-1} s, which is more than one order of magnitude smaller than the allowed values of 2-5 s for assuming saturation adjustment (Thouron et al., 2012). The present case hence is an ideal environment evaluating the error introduced by using saturation adjustment and by keeping all other parameters the same.

Atmos. Chem. Phys. Discuss., https://doi.org/10.5194/acp-2018-1139
Manuscript under review for journal Atmos. Chem. Phys.
Discussion started: 6 November 2018

Atmospheric Chemistry and Physics Discussions

Figure 3 shows time series of the saturation (supersaturation) for REF and C1 case. In both cases saturation occurs simultaneously around 0100 UTC. In case REF, relative humidity does not exceed 100% due to its limitation by saturation adjustment, while in case C1 maximum supersaturations of 0.12% occur, which corresponds to typical values within fog. For example, in the simulations of both Mazoyer et al. (2017) and Boutle et al. (2018) values close to 0.1% were observed, and in-situ observations during the ParisFog experiment revealed supersaturations of 0.05% (Hammer et al., 2014).

Case C1 also shows that the supersaturation reaches its maximum at 0345 UTC and persists until 0700 UTC. At 2 m and 20 m height, however, supersaturation is in the range of 0.05%. Starting from 0350 UTC and 0315 UTC, respectively, supersaturations are removed and the air becomes subsaturated. This is in contrast with case REF where the saturation adjustment approach keeps the relative humidity at 100% as long as liquid water is present (i.e. until the fog has dissipated). Around 0600 UTC, which is shortly after sunrise, relative humidity drops rapidly as a direct consequence of solar radiation heating the surface and the near-surface air, preventing further supersaturation at these heights. While we cannot clearly identify the lifting of the fog in case C1 (due to the limited humidity range displayed), we note that for case REF we can identify lifting times as a decrease of relative humidity around 0845 UTC at 2 m height and around 0910 UTC at 20 m height.

Beside this inherent difference in relative humidity, the general time marks (formation, lifting, dissipation, defined as in Maronga and Bosveld (2017)) of the fog layer are very similar for cases REF and C1. This allows a direct comparison of both cases.

In Fig. 4 the total difference of the liquid water mixing ratio q_l (REF minus C1) is shown. A clear tendency can be seen in the liquid water difference: On the top of the fog, where the highest supersaturation occurs due to radiative cooling, the largest differences in q_l of up to 0.06 g kg^{-1} can be observed (negative difference, blue). In general, the REF case shows higher values for q_l during the formation and mature phase of the fog. Close to the bottom where the net condensation is low (between 0400 UTC and 0600 UTC), the differences for q_l diminishes. Only in a few upper levels during lifting at a height of 240 m the C1 case exhibits higher liquid water mixing ratios.

This finding is directly linked to the used condensation schemes. The saturation adjustment scheme (REF) converts all excess moisture into liquid water. As long as diffusional growth (calculated via saturation adjustment) has a positive tendency, q_l will thus have higher values compared to case C1.

Figure 5 shows the liquid water path (LWP) for both cases. Differences in the LWP appear between 0400 UTC and 1100 UTC and are up to 6.9% (lower values for case C1). Simulations with a coarser grid spacing of 4 m (not shown), which result in a larger time step (approximately 0.6 s) for the same setup, exhibit nearly no differences for the different condensation schemes. As mentioned earlier and in previous publications the use of saturation adjustment is always a question of the time scales to be considered. This suggests that the effect of saturation adjustment on the integrated water content is negligible for simulations with sufficiently long time steps, but will lead to greater errors with decreasing time step. However, it can be summarized that, although the assumptions of saturation adjustment have no validity for the simulation of fog when using a very small time step, and the mean liquid water content is changed by nearly 7%, the general fog structure remains unaffected. We suppose that this finding is due to the very small supersaturation, which is not strong enough to generate a significant change in the effective radius which could lead to stronger sedimentation or an overall increased optical depth.

Atmos. Chem. Phys. Discuss., https://doi.org/10.5194/acp-2018-1139
Manuscript under review for journal Atmos. Chem. Phys.
Discussion started: 6 November 2018

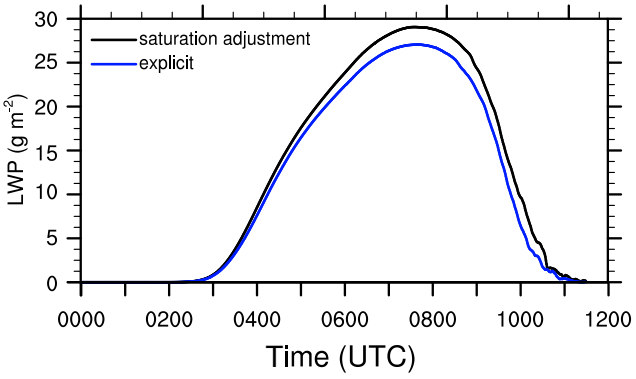

Figure 5. Liquid water path (LWP) of reference case REF using the saturation adjustment scheme and C1 case using an explicit calculation of diffusional growth.

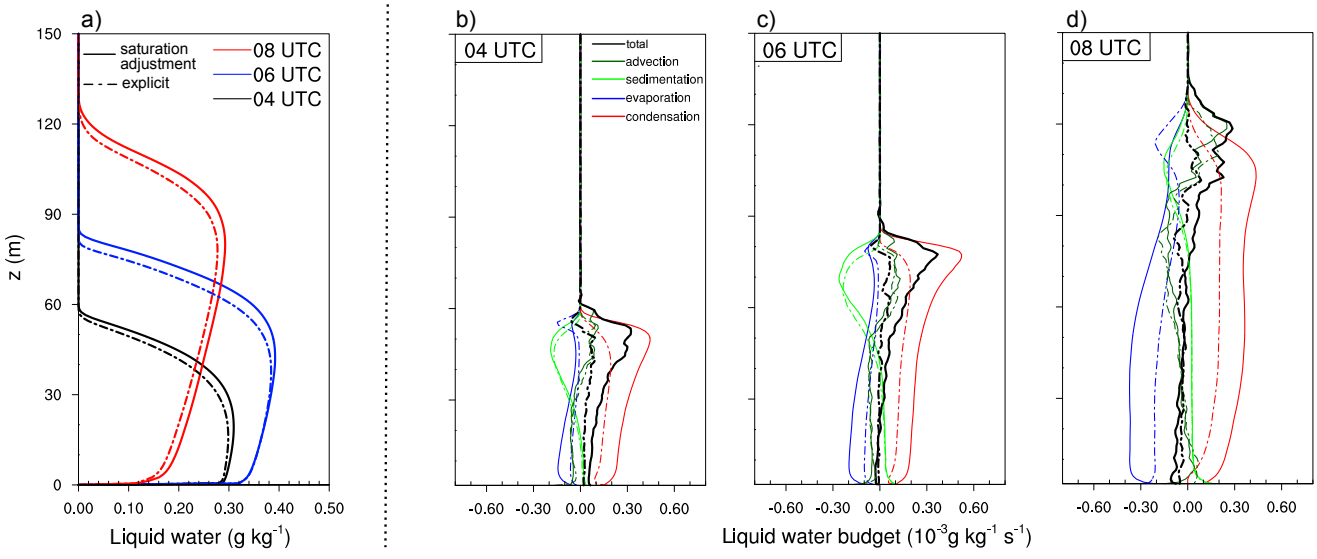

Figure 6. Instantaneous horizontally averaged profiles for the liquid water mixing ratio (a) for 0400 UTC, 0600 UTC and 0800 UTC and budgets for q_l tendencies (b-d) for 0400 UTC, 0600 UTC and 0800 UTC for the simulations REF and C1.

Fig. 6 shows profiles for the liquid water mixing ratio (a) as well as the liquid water budgets (b-d) at 0400 UTC, 0600 UTC and 0800 UTC for cases REF and C1. These times represent different stages of the fog development: deepening, mature phase, and mature phase development after sunrise, respectively. Figure 6a confirms that especially at the top of the fog, when it becomes radiatively active, the liquid water is overestimated in the case of saturation adjustment. Figures 6b-d show a clear trend: On the one hand the sedimentation and advection rates are almost identical for both cases at all times. On the other hand, clear differences can be observed in the production rate for condensation and the dissipation rate due to evaporation. In the case of saturation adjustment, these rates are almost twice as high (in absolute sense) as for the C1 case over the entire

Atmos. Chem. Phys. Discuss., https://doi.org/10.5194/acp-2018-1139
Manuscript under review for journal Atmos. Chem. Phys.
Discussion started: 6 November 2018

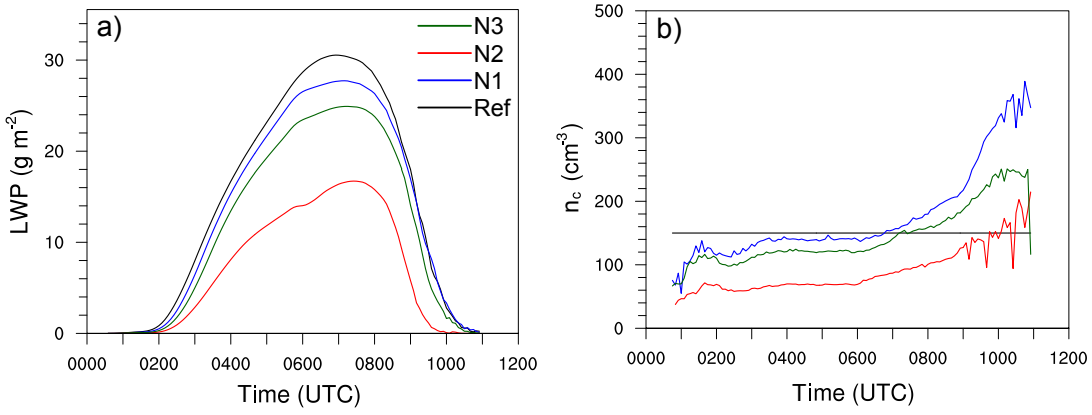

Figure 7. Time series of LWP and n_c for the reference and N1-N3 case.

height of the fog layer. This finding can be attributed to the fact that saturation adjustment is assuming the highest possible values for condensation. This in turn also affects the evaporation rates, which are counteracting the production by excessive condensation. The net effect, however, is comparatively small. Interestingly, it can be observed that the condensation rates are significantly higher towards the top of the fog when using saturation adjustment. This agrees with the previous finding from Fig. 4 that more liquid water is found in the upper part of the fog layer in case REF. This can be explained by the fact that the excessive condensation at the upper edge is caused by radiation cooling, which itself is proportional to the available liquid water content. This leads to a non-linear positive feedback mechanism, where the overestimation of condensation rates of the saturation adjustment scheme inherently produces too high values for q_l, which in turn is increasing radiative cooling and hence producing new supersaturations which again are converted too fast into liquid water.

4.3 Comparison of different activation parameterizations

In numerous previous studies, the influence of aerosols and the activation process on the life cycle of fog was investigated (e.g. Bott, 1991; Stolaki et al., 2015; Maalick et al., 2016; Zhang et al., 2014; Boutle et al., 2018). Although all three activation schemes are comparable power law parameterizations that are initialized with identical aerosol spectra, the influence on the fog is still to be investigated, since the n_c has a significant influence on the life cycle of fog and thus also small differences of the schemes can cause significant feedbacks.

Furthermore, n_c as a function of time is shown in Fig. 7b for the reference case and cases N1-N3, representing runs with the three different aerosol activation parameterization schemes (see Tab.1). The quantitative differences in the number of activated aerosol by using the different activation schemes is explained by a slightly different activation spectrum (see Appendix, Fig. A1). In principle, a similar qualitative development of n_c can be observed. While n_c increases during fog formation, it remains nearly constant during the mature phase of the fog for all cases. This can be explained by a constant longwave cooling at the fog top, producing unvarying maximum supersaturations. However, as soon as the sun rises and the fog layers start to lift, all cases show a strong increase in the n_c. This increase can be explained by stronger supersaturations induced by thermal

Atmos. Chem. Phys. Discuss., https://doi.org/10.5194/acp-2018-1139
Manuscript under review for journal Atmos. Chem. Phys.
Discussion started: 6 November 2018

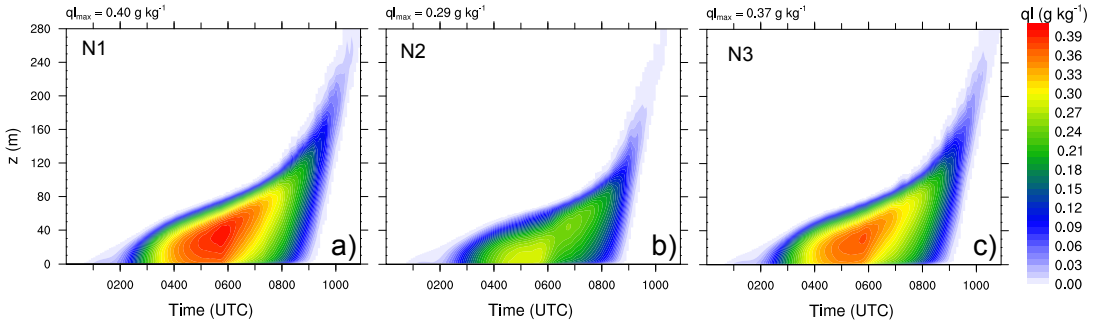

Figure 8. Height-time cross sections for the liquid water mixing ratio for N1-N3.

updrafts in the developing surface-driven convective boundary layer due to surface heating by solar radiation. Moreover, we note that while the qualitative course of n_c is similar for all cases, the choice of the activation algorithm has an impact on number of activated aerosol and thus on the strength of the fog-layer (see Fig. 8). Time series of the LWP for the reference run and the three different cases are shown in Fig. 7a. The highest LWP occurs for the reference run which also shows the highest n_c during the formation and mature phase in comparison with the other simulations. Also for the cases N1-N3 a linear relationship between LWP and n_c can be found: A higher n_c leads to higher LWP. On the one hand, this is due to the radiation effect of the droplets. The number of droplets to which a certain amount of liquid water is distributed plays an important role. The larger the number of droplets, the larger is the radiation-effective surface and thus also the optical thickness. As a result, the cooling rate from a fog with many small droplets is increased, allowing more water vapor to condense and the fog to grow more strongly. On the other hand, also sedimentation plays a major role which is discussed in the following.

Figure 9a shows the profiles of the liquid water mixing ratio at 0400 UTC, 0600 UTC, and 0800 UTC. Here, it can be seen that the cases with higher values of q_l, integrated over the entire height, also contain most liquid water throughout the fog layer. The maximum q_l in the fog layer is reached at approximately 0600 UTC at a height of 60 m. Afterwards a further vertical growth of the fog can be observed, where no further increase in liquid water takes places as a result of larger vertical extent of the mixing layer and due to rising temperatures after sunrise (see Fig. 6a). Moreover, Fig. 9b,c shows the liquid water budget at 0600 UTC, when the fog was fully developed. Almost all three cases shows identical values for condensation rates (see Fig. 9b) in the lowest part of the fog layer, with values being in the same order as the evaporation rates, so that the net gain in this region appears to be negligible. However, the N2 case (with the lowest n_c) exhibits a generally lower absolute evaporation rate compared to both other cases, which is explained by slightly higher mean values of the relative humidity (not shown) than in N1 and N3. In the upper part of the fog layer higher values of the condensation rate are observed (especially for N1 and N3) with a concurrent decrease in evaporation rates, displaying the deepening of the fog layer. At a height of approximately 80 m a maximum of the evaporation rates can be observed, representing the presence of subsaturated regions in this height and the top of the fog. Larger differences can be observed in the sedimentation rates: First and foremost the sedimentation is proportional to the liquid water mixing ratio (see also Eq. 3). However, the strength of sedimentation also depends on the mean radius of the droplets, which increases with decreasing number of activated drops. Here, a lower n_c for a given amount

of liquid water leads to a higher mean radius, compared to a higher n_c where the same amount of water is distributed to more drops, decreasing the mean radius. Integrated over height all three cases exhibit approximately the same sedimentation rates. Therefore, case N2 suffers the most from the loss of liquid water due to sedimentation (in relative terms). Moreover, Fig. 9c shows that sedimentation partially counteracts the gains caused by condensation at the upper edge of the fog. All in all it can be summarized that all shown processes affect the net change of the liquid water mixing ratio. However, in the mature phase sedimentation plays a key role, showing the highest values for the individual tendencies. As a result liquid water is slowly and constantly removed from the fog layer. These findings are in good agreement with investigations by Bott (1991). The sum of all tendencies is the height-dependent change of the liquid water. Also here it can be seen that in the lower 50 m the net tendency is negative, while in higher levels we observe a positive tendency, so that the fog continues growing vertically.

Figure 10a shows profiles of n_c at 0400 UTC, 0600 UTC and 0800 UTC. We see that the profiles of the different cases differ quantitatively but not qualitatively. The stage of the fog can thus be identified in the profiles for all cases: At 0400 UTC highest supersaturations occur close to the ground due to cooling of the surface and near-surface air, leading to high activation rates and therefore high n_c near the surface. At 0600 UTC a well-mixed layer has developed that is driven by the radiative cooling from the fog-top. While the turbulent mixing leads to a vertical well-mixed n_c, we note the maximum at the top, where the radiative cooling induces immense aerosol activation. This is also displayed in the budget of the n_c (see Fig. 10b,c), where the instantaneous rates for 0600 UTC are shown. Here, we see clearly that aerosol activation at the top of the fog layer is the dominant process in the mature phase of the fog, while activation near the surface is relatively unimportant. Also, we see that both, advection and sedimentation are much less important than activation. Finally, we note that deactivation, while being small, does occur at the fog top, reflecting updrafts of foggy air penetrating the subsaturated air aloft.

Atmos. Chem. Phys. Discuss., https://doi.org/10.5194/acp-2018-1139
Manuscript under review for journal Atmos. Chem. Phys.
Discussion started: 6 November 2018

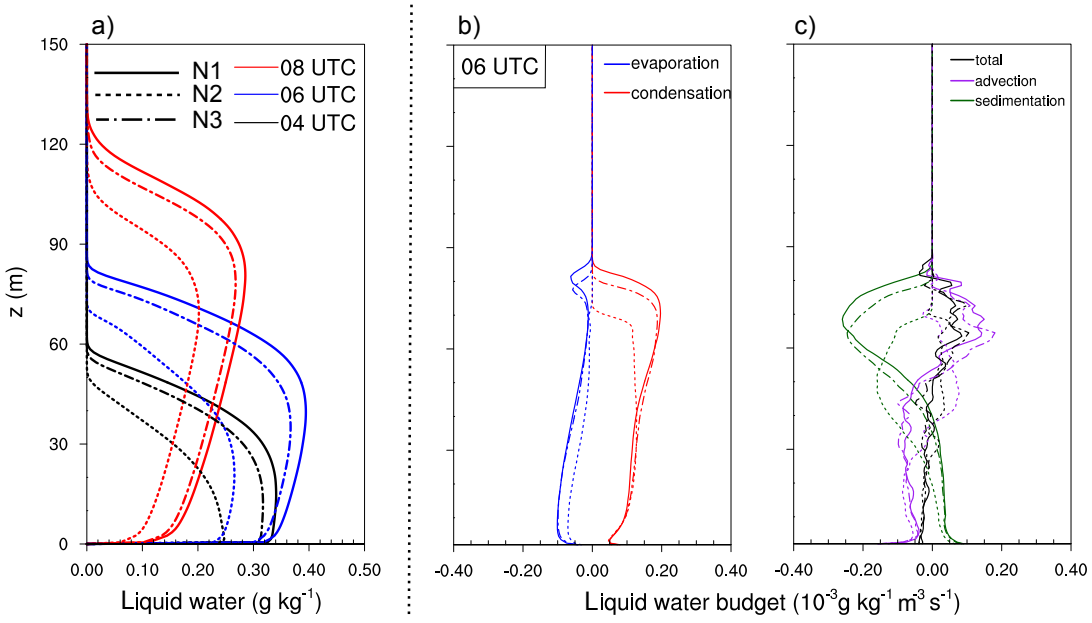

Figure 9. Profiles (instantaneously and horizontally averaged) of liquid water mixing ratio at 0400 UTC, 0600 UTC and 0800 UTC and profiles of explicit liquid water budget terms at 0600 UTC.

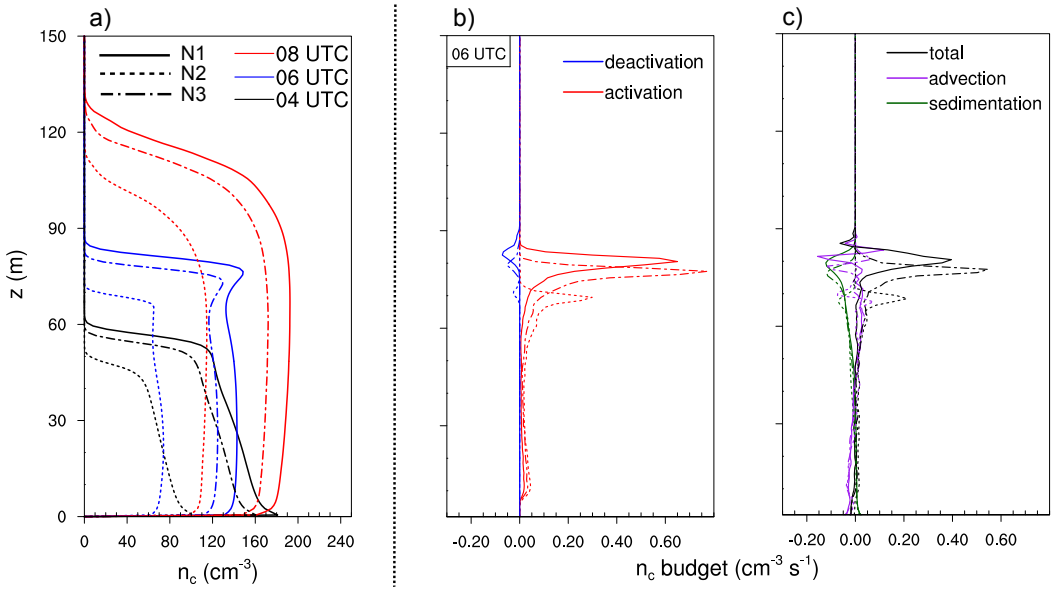

Figure 10. Profiles (instantaneously and horizontally averaged) of n_c at 0400 UTC, 0600 UTC and 0800 UTC and profiles of explicit n_c budget terms at 0600 UTC.

Atmos. Chem. Phys. Discuss., https://doi.org/10.5194/acp-2018-1139
Manuscript under review for journal Atmos. Chem. Phys.
Discussion started: 6 November 2018

5 Conclusions

The main objective of this work was to investigate the influence of the choice of the microphysical parameterization used in LES models on the life cycle of simulated nocturnal radiation fog. For this purpose we performed a series of LES runs for a well-known fog event observed at Cabauw (Netherlands). First, we compared the possible error introduced when using saturation adjustment in comparison with the explicit representation of diffusional growth. The results showed that, although the model time step was inappropriate for the assumptions made during saturation adjustment, the differences in LWP are at most 6.9% and the general life cycle was not affected. This could be attributed to the fact that the typical supersaturations in fog are in the range of a few tenths of a percent, and the resulting absolute differences are too small to induce a further influence on dynamics, microphysics or radiation. However, when looking in more detail, we found that the LES run with saturation adjustment produced higher liquid water mixing ratios in comparison to a comparative run using the explicit scheme for the whole fog layer with the largest differences at the fog top, caused by excessive condensation due to radiative cooling. These supersaturations are removed immediately by using the saturation adjustment scheme, leading to an overestimation of the liquid water mixing ratios, and due to a positive feedback mechanism to stronger radiative cooling and again to more liquid water content.

In a second part of our study, the effect of different activation schemes of Twomey (1959), Cohard et al. (1998) and Khvorostyanov and Curry (2006) on the simulated fog life cycle were investigated (cases N1 to N3). Even though these parameterizations are very similar, our results indicate that the number of activated aerosols (and consequently the number of droplets) are a crucial parameter for the fog development and differed significantly. An analysis of the budgets of n_c and q_l showed that diffusional growth is the major process for generating liquid water, but was found to be independent of the number of droplets and thus comparable in magnitude in all cases. In contrast, the sedimentation rates showed a different behaviour: On the one hand, these were found to be proportional to the liquid water mixing ratio, which is high in cases N1 and N3. On the other hand, the sedimentation depends on the mean radius of the droplets, which is higher in the case of fewer activated aerosols (case N2). Overall, this leads to almost identical absolute integral sedimentation rate for the three schemes. However, this means that liquid water is removed by sedimentation more rigorously in case N2 (in relative terms) compared to cases N1 and N3. Moreover, we could show that most aerosol activation happens near the surface during the formation phase of the fog, while the maximum number of activated aerosols during the mature phase is located at the top of the fog layer. The latter results from the radiative cooling of the fog top, producing the largest supersaturations. However, this radiative cooling triggers a top-down convective layer, so that the the droplets are well mixed, leading to an evenly distributed number concentration throughout the fog layer.

In summary, the present study indicates that the choice of the used microphysics parameterization can be a key factor for the simulation of radiation fog. At the moment, however, we have no means to give advice on which parameterization performs best. In order to overcome these limitations of the present study, we plan to revisit this particular fog case using a Lagrangian particle-based approach to simulate the microphysics of droplets which will allow for explicitly simulating the development of the 3D droplet size distribution in the fog layer (e.g. Shima et al., 2009). This approach will also allow to resolve all relevant

microphysical processes such as activation and diffusional growth instead of parameterizing them. As such simulations are computationally very expensive, only a very limited number of simulations are feasible at the moment, so that most future numerical investigations will - as in the present work - rely on bulk microphysics parameterizations. Based on the results using the Lagrangian approach, however, we hope to be able to give an educated recommendation on the best choice for such bulk parameterizations.

Code availability. The PALM model used in this study (revision 2675) is publicly available on http://palm-model.org/trac/browser/palm?rev=2675. For analysis, the model has been extended and additional analysis tools have been developed. The extended code is available from the authors on request.

Atmos. Chem. Phys. Discuss., https://doi.org/10.5194/acp-2018-1139
Manuscript under review for journal Atmos. Chem. Phys.
Discussion started: 6 November 2018

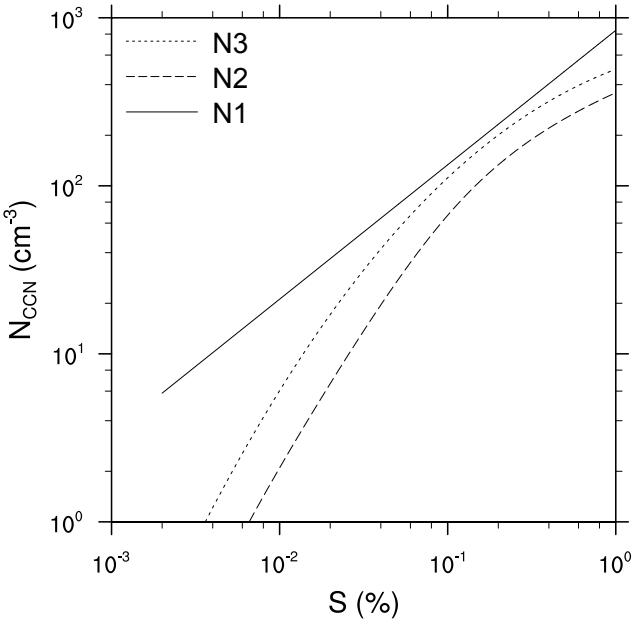

Figure A1. Activation spectrum for three different activation schemes of Twomey (1959)(N1), Cohard et al. (1998)(N2) and Khvorostyanov and Curry (2006)(N3).

Appendix A: Activation spectrum

In Fig. A1 the activation spectrum for the three different activation schemes of Twomey (1959) (N1), Cohard et al. (1998) (N2) and Khvorostyanov and Curry (2006) (N3) are shown.

Author contributions. JS and MB designed the numerical experiments and JS carried them out and made the analysis. JS and BM developed the basic ideas, discussed the results, and wrote the manuscript.

Competing interests. The authors declare that they have no conflict of interest.

Acknowledgements. This work has been funded by the German Research Foundation (DFG) under Grant MA 6383/1-1, which is greatly acknowledged. All simulations have been carried out on the Cray XC-40 systems of the North-German Supercomputing Alliance (HLRN, https://www.hlrn.de/).

References

Abdul-Razzak, H. and Ghan, S. J.: A parameterization of aerosol activation: 2. Multiple aerosol types, J. Geophys. Res. Atmos., 105, 6837–6844, 2000.

Ackerman, A. S., VanZanten, M. C., Stevens, B., Savic-Jovcic, V., Bretherton, C. S., Chlond, A., Golaz, J.-C., Jiang, H., Khairoutdinov, M., Krueger, S. K., et al.: Large-eddy simulations of a drizzling, stratocumulus-topped marine boundary layer, Mon. Weather Rev., 137, 1083–1110, 2009.

Árnason, G. and Brown Jr, P. S.: Growth of cloud droplets by condensation: A problem in computational stability, J. Atmos. Sci., 28, 72–77, 1971.

Beare, R. J., Macvean, M. K., Holtslag, A. A., Cuxart, J., Esau, I., Golaz, J.-C., Jimenez, M. A., Khairoutdinov, M., Kosovic, B., Lewellen, D., et al.: An intercomparison of large-eddy simulations of the stable boundary layer, Boundary-Layer Meteorol., 118, 247–272, 2006.

Bergot, T.: Small-scale structure of radiation fog: a large-eddy simulation study, Quart. J. Roy. Meteor. Soc., 139, 1099–1112, 2013.

Boers, R., Baltink, H. K., Hemink, H., Bosveld, F., and Moerman, M.: Ground-based observations and modeling of the visibility and radar reflectivity in a radiation fog layer, J. Atmos. Ocean Technol., 30, 288–300, 2013.

Bott, A.: On the influence of the physico-chemical properties of aerosols on the life cycle of radiation fogs, Boundary-Layer Meteorol., 56, 1–31, 1991.

Bott, A. and Trautmann, T.: PAFOG—a new efficient forecast model of radiation fog and low-level stratiform clouds, Atmos. Res., 64, 191–203, 2002.

Bougeault, P.: Modeling the trade-wind cumulus boundary layer. Part I: Testing the ensemble cloud relations against numerical data, J. Atmos. Sci., 38, 2414–2428, 1981.

Boutle, I., Price, J., Kudzotsa, I., Kokkola, H., and Romakkaniemi, S.: Aerosol-fog interaction and the transition to well-mixed radiation fog, Atmos. Chem. Phys., 18, 7827–7840, 2018.

Clough, S. A., Shephard, M. W., Mlawer, E. J., Delamere, J. S., Iacono, M. J., Cady-Pereira, K., Boukabara, S., and Brown, P. D.: Atmospheric radiative transfer modeling: A summary of the AER codes, Short Communication, J. Quant. Spectrosc. Radiat. Transfer, 91, 233–244, 2005.

Cohard, J.-M. and Pinty, J.-P.: A comprehensive two-moment warm microphysical bulk scheme. I: Description and tests, Quart. J. Roy. Meteor. Soc., 126, 1815–1842, 2000.

Cohard, J.-M., Pinty, J.-P., and Bedos, C.: Extending Twomey's analytical estimate of nucleated cloud droplet concentrations from CCN spectra, J. Atmos. Sci., 55, 3348–3357, 1998.

Geoffroy, O., Brenguier, J.-L., and Sandu, I.: Relationship between drizzle rate, liquid water path and droplet concentration at the scale of a stratocumulus cloud system, Atmos. Chem. Phys., 8, 4641–4654, 2008.

Geoffroy, O., Brenguier, J.-L., and Burnet, F.: Parametric representation of the cloud droplet spectra for LES warm bulk microphysical schemes, Atmos. Chem. Phys., 10, 4835–4848, 2010.

Grabowski, W. W. and Morrison, H.: Toward the mitigation of spurious cloud-edge supersaturation in cloud models, Mon. Weather Rev., 136, 1224–1234, 2008.

Gultepe, I., Tardif, R., Michaelides, S., Cermak, J., Bott, A., Bendix, J., Müller, M. D., Pagowski, M., Hansen, B., Ellrod, G., et al.: Fog research: A review of past achievements and future perspectives, in: Fog and Boundary Layer Clouds: Fog Visibility and Forecasting, pp. 1121–1159, Springer, 2007.

Gultepe, I., Hansen, B., Cober, S., Pearson, G., Milbrandt, J., Platnick, S., Taylor, P., Gordon, M., and Oakley, J.: The fog remote sensing and modeling field project, Bulletin of the American Meteorological Society, 90, 341–359, 2009.

Haeffelin, M., Bergot, T., Elias, T., Tardif, R., Carrer, D., Chazette, P., Colomb, M., Drobinski, P., Dupont, E., Dupont, J.-C., et al.: PARIS-FOG: shedding new light on fog physical processes, Bulletin of the American Meteorological Society, 91, 767–783, 2010.

Hammer, E., Gysel, M., Roberts, G., Elias, T., Hofer, J., Hoyle, C., Bukowiecki, N., Dupont, J.-C., Burnet, F., Baltensperger, U., et al.: Size-dependent particle activation properties in fog during the ParisFog 2012/13 field campaign, Atmos. Chem. Phys., 14, 10 517–10 533, 2014.

Heus, T., Van Heerwaarden, C., Jonker, H. J., Siebesma, A. P., Axelsen, S., Van Den Dries, K., Geoffroy, O., Moene, A., Pino, D., De Roode, S., et al.: Formulation of the Dutch Atmospheric Large-Eddy Simulation (DALES) and overview of its applications, Geosci. Model Dev., 3, 415, 2010.

Khairoutdinov, M. and Kogan, Y.: A new cloud physics parameterization in a large-eddy simulation model of marine stratocumulus, Mon. Weather Rev., 128, 229–243, 2000.

Khvorostyanov, V. I. and Curry, J. A.: Aerosol size spectra and CCN activity spectra: Reconciling the lognormal, algebraic, and power laws, J. Geophys. Res. Atmos., 111, 2006.

Lebo, Z. J., Morrison, H., and Seinfeld, J. H.: Are simulated aerosol-induced effects on deep convective clouds strongly dependent on saturation adjustment?, Atmos. Chem. Phys., 12, 9941–9964, 2012.

Maalick, Z., Kühn, T., Korhonen, H., Kokkola, H., Laaksonen, A., and Romakkaniemi, S.: Effect of aerosol concentration and absorbing aerosol on the radiation fog life cycle, Atmos. Environ., 133, 26–33, 2016.

Maronga, B. and Bosveld, F.: Key parameters for the life cycle of nocturnal radiation fog: a comprehensive large-eddy simulation study, Quart. J. Roy. Meteor. Soc., 2017.

Maronga, B., Gryschka, M., Heinze, R., Hoffmann, F., Kanani-Sühring, F., Keck, M., Ketelsen, K., Letzel, M. O., Sühring, M., and Raasch, S.: The Parallelized Large-Eddy Simulation Model (PALM) version 4.0 for atmospheric and oceanic flows: model formulation, recent developments, and future perspectives, Geosci. Model Dev., 2015.

Mazoyer, M., Lac, C., Thouron, O., Bergot, T., Masson, V., and Musson-Genon, L.: Large eddy simulation of radiation fog: impact of dynamics on the fog life cycle, Atmos. Chem. Phys., 17, 13 017, 2017.

Mensah, A., Holzinger, R., Otjes, R., Trimborn, A., Mentel, T. F., Brink, H. t., Henzing, B., and Kiendler-Scharr, A.: Aerosol chemical composition at Cabauw, The Netherlands as observed in two intensive periods in May 2008 and March 2009, Atmos. Chem. Phys., 12, 4723–4742, 2012.

Morrison, H. and Grabowski, W. W.: Comparison of bulk and bin warm-rain microphysics models using a kinematic framework, J. Atmos. Sci., 64, 2839–2861, 2007.

Morrison, H. and Grabowski, W. W.: Modeling supersaturation and subgrid-scale mixing with two-moment bulk warm microphysics, J. Atmos. Sci., 65, 792–812, 2008.

Nakanishi, M.: Large-eddy simulation of radiation fog, Boundary-Layer Meteorol., 94, 461–493, 2000.

Pruppacher, H. R. and Klett, J. D.: Microphysics of clouds and precipitation, Kluwer Academic Publishers, Dordrecht, Netherlands, 2nd revised edn., 1997.

Seifert, A. and Beheng, K. D.: A double-moment parameterization for simulating autoconversion, accretion and selfcollection, Atmos. Res., 59, 265–281, 2001.

Seifert, A., Khain, A., Pokrovsky, A., and Beheng, K. D.: A comparison of spectral bin and two-moment bulk mixed-phase cloud microphysics, Atmos. Res., 80, 46–66, 2006.

Shima, S., Kusano, K., Kawano, A., Sugiyama, T., and Kawahara, S.: The super-droplet method for the numerical simulation of clouds and precipitation: A particle-based and probabilistic microphysics model coupled with a non-hydrostatic model, Quart. J. Roy. Meteor. Soc., 135, 1307–1320, 2009.

Stolaki, S., Haeffelin, M., Lac, C., Dupont, J.-C., Elias, T., and Masson, V.: Influence of aerosols on the life cycle of a radiation fog event. A numerical and observational study, Atmos. Res., 151, 146–161, 2015.

Thouron, O., Brenguier, J.-L., and Burnet, F.: Supersaturation calculation in large eddy simulation models for prediction of the droplet number concentration, Geosci. Model Dev., 5, 761–772, 2012.

Twomey, S.: The nuclei of natural cloud formation part II: The supersaturation in natural clouds and the variation of cloud droplet concentration, Pure Appl. Geophys., 43, 243–249, 1959.

Zhang, X., Musson-Genon, L., Dupont, E., Milliez, M., and Carissimo, B.: On the influence of a simple microphysics parametrization on radiation fog modelling: A case study during parisfog, Boundary-Layer Meteorol., 151, 293–315, 2014.